Electronic Supplementary Material (ESI) for Journal of Materials Chemistry A.
This journal is © The Royal Society of Chemistry 2020

Supporting Information

# Silicothermic Reduction Reaction for Fabricating Interconnected Si-Ge Nanocrystals with Fast and Stable Li-Storage

Jie Zhou,†[a] Haoyu Zhao,†[a] Ning Lin,*[a] Tieqiang Li,[a] Yang Li,[a] Song Jiang,[a] Jie Tian,[a] Yitai Qian*[a]

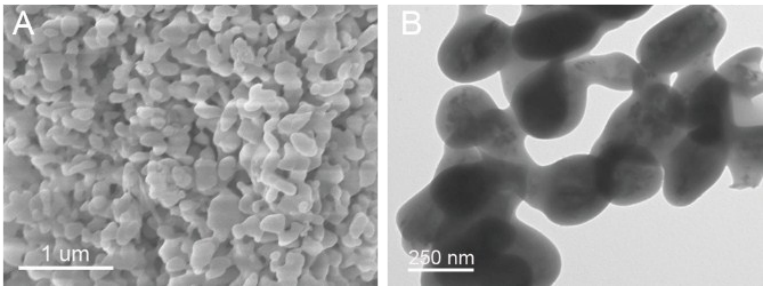


**Fig. S1** SEM and TEM images of SG-4 nanocomposites.

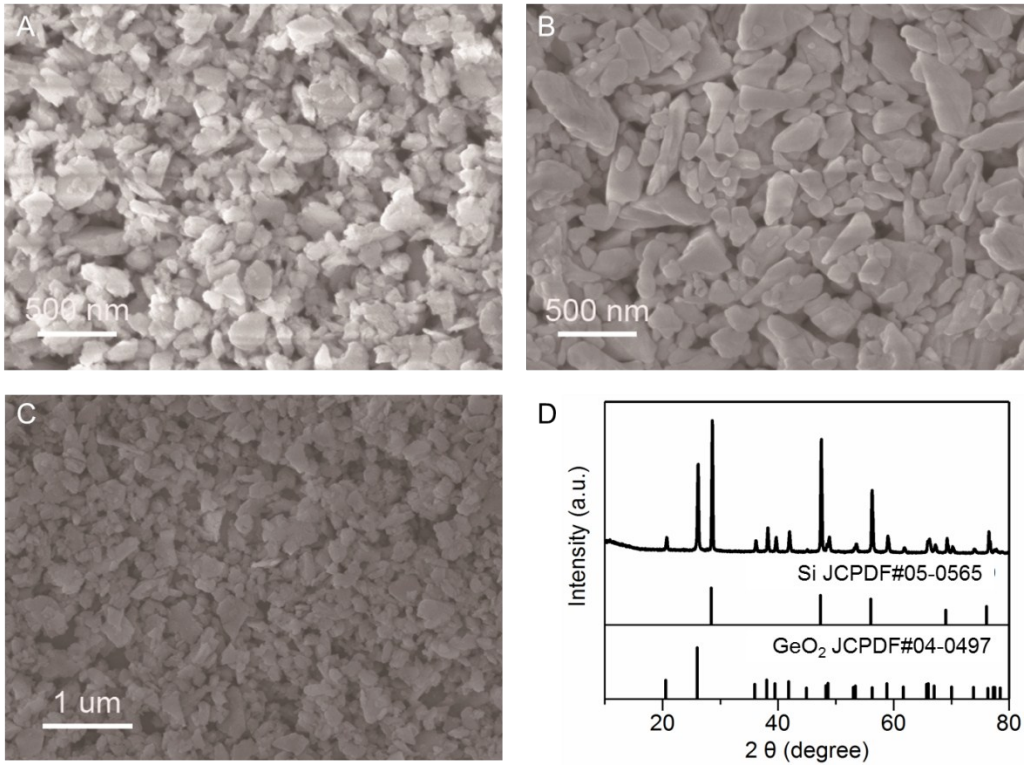


**Fig. S2** Characterization of the precursor of Si and $GeO_2$. SEM image of (A) Si, (B) $GeO_2$ and (C) mixing composite of Si and $GeO_2$. (D) XRD pattern of the mixing composite of Si and $GeO_2$.

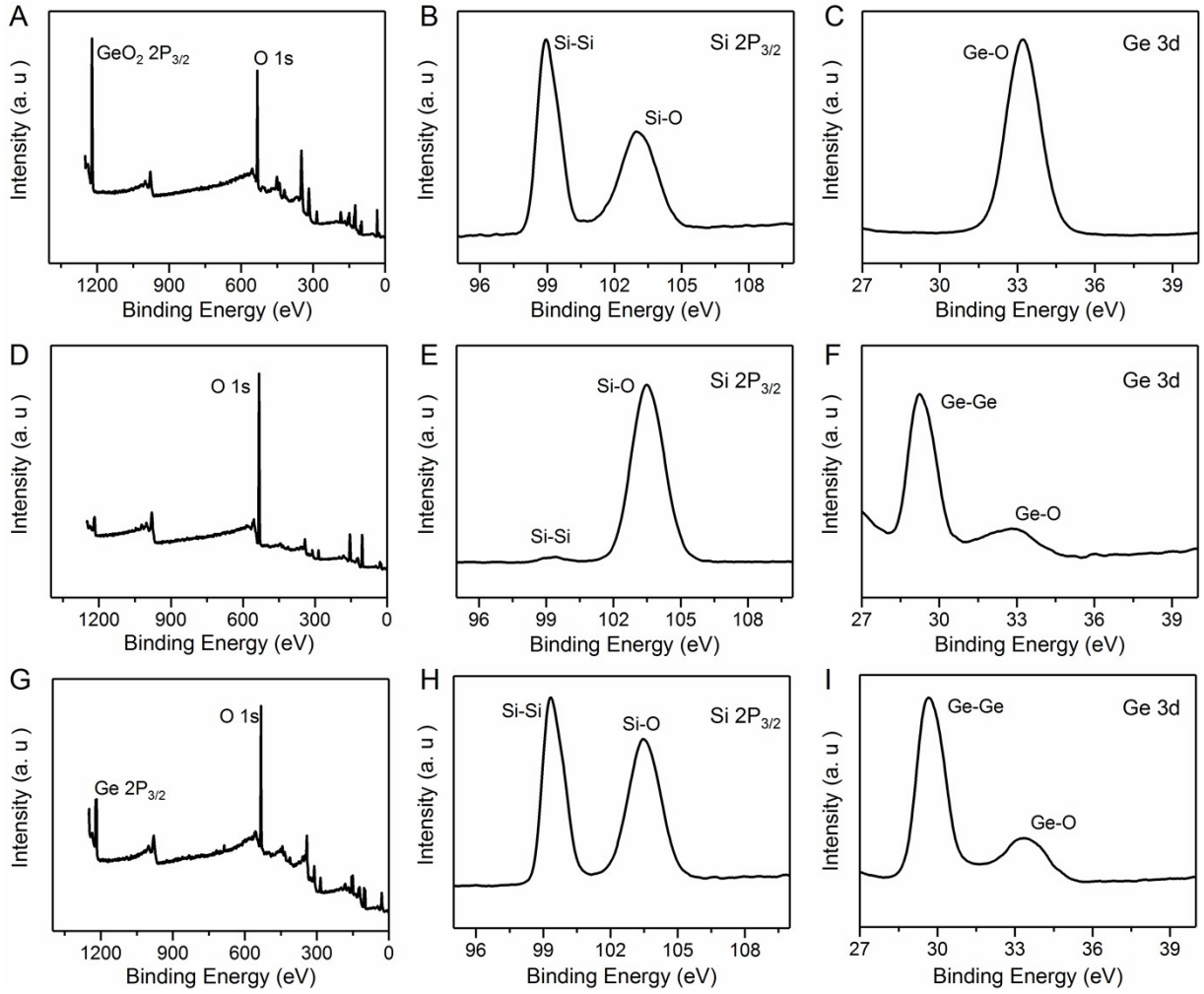


**Fig. S3** Chemical States changes of Si and Ge during silicothermic reduction process. (A) XPS total spectrum (B) core-level Si $2p_{3/2}$ and (C) Ge 3d of Si-$GeO_2$ composites before silicothermic reduction reaction. (D) XPS total spectrum (E) core-level Si $2p_{3/2}$ and (F) Ge 3d of Si-Ge nanocomposites after silicothermic reduction reaction. (G) XPS total spectrum (H) core-level Si $2p_{3/2}$ and (I) Ge 3d of Si-Ge nanocomposites after washed with HF.

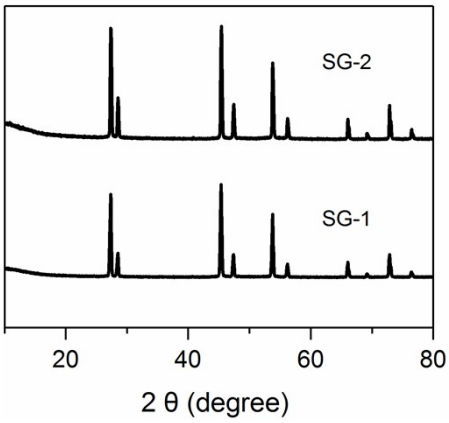


**Fig. S4** XRD pattern of the other two Si/Ge nanocomposites (SG-2 and SG-1).

**Table S1**. Changes of entropy and enthalpy of Si, $GeO_2$, Ge and $SiO_2$ at 298 K.

| T=298 K | Si | $GeO_2$ | Ge | $SiO_2$ |
|---|---|---|---|---|
| $\Delta H$ (J $mol^{-1}$) | 0 | -558351 | 0 | -910857 |
| $\Delta S$ (J $mol^{-1}$) | 18.828 | 55.271 | 31.087 | 41.463 |

$\Delta H$ and $\Delta S$ is the Changes of enthalpy and entropy, respectively.

**Table S2**. Changes of entropy and enthalpy of Si, $GeO_2$, Ge and $SiO_2$ at 1100 K.

| T=1100 K | Si | $GeO_2$ | Ge | $SiO_2$ |
|---|---|---|---|---|
| $\Delta H$ (J $mol^{-1}$) | 19586 | -501903 | 20603 | -858584 |
| $\Delta S$ (J $mol^{-1}$) | 49.861 | 143.917 | 64.117 | 122.613 |

$\Delta H$ and $\Delta S$ is the Changes of enthalpy and entropy, respectively.

$$\Delta H=-858584+20603+501903-19586=-355664 \text{ J mol}^{-1}$$

$$\Delta S=122.613+64.117-143.917-49.861=-7.048 \text{ J mol}^{-1}$$

$$\Delta G=H-TS=-355664-1100*(-7.048)=-347911.2 \text{ J mol}^{-1}$$

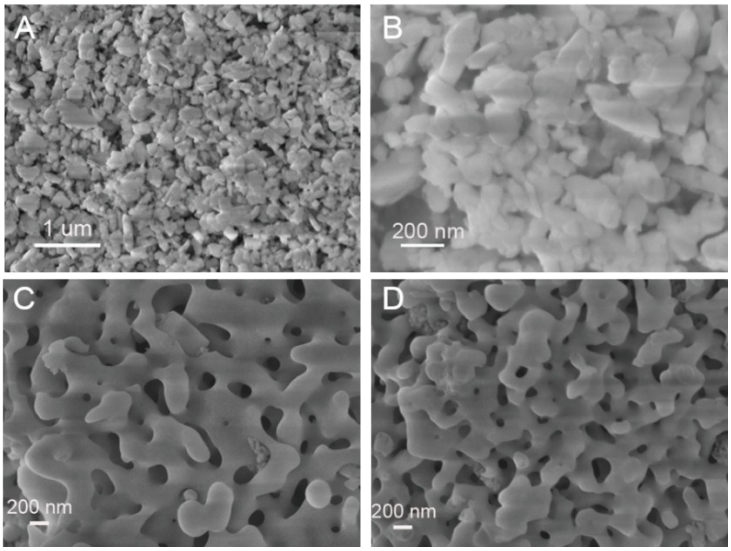


**Fig. S5** SEM images of (A-B) Si-Ge nanocomposites with the molar ratio of 4:1 obtained via the silicothermic reduction without $ZnCl_2$. (C) SG-2 and (D) SG-1 nanocrystal obtained via the silicothermic reduction with $ZnCl_2$.

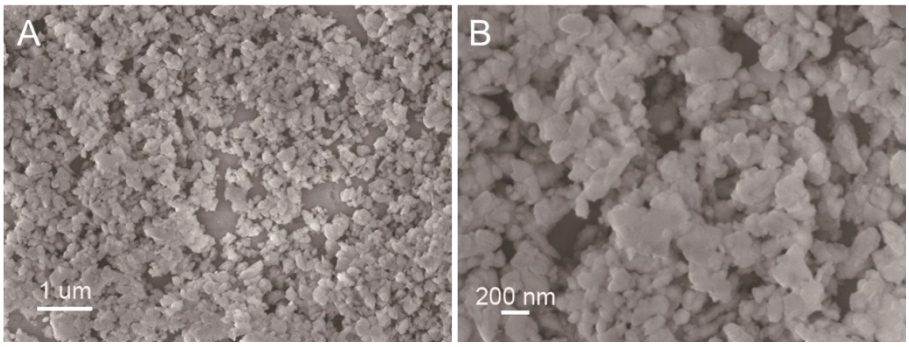


**Fig. S6** SEM images of $Cu_3Si$/Cu@Si nanocomposites.

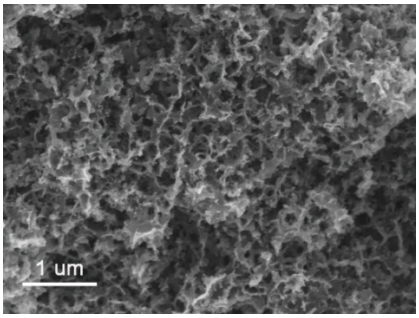


**Fig. S7** SEM image of Si-C nanocomposites.

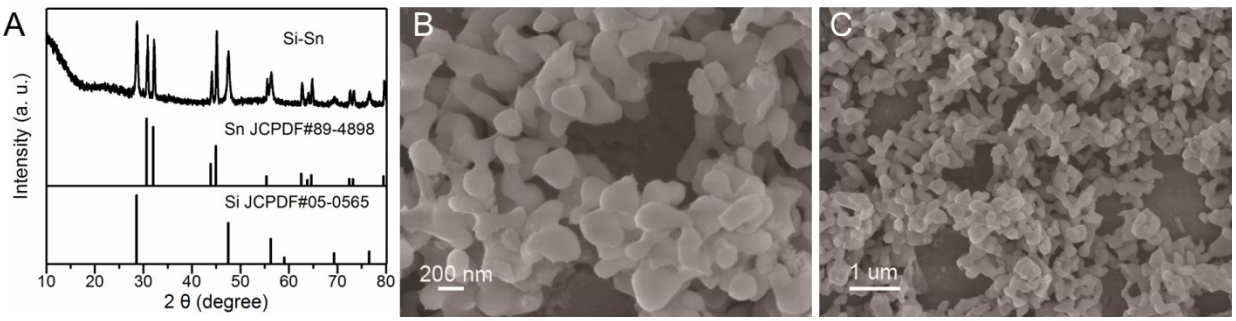


**Fig. S8** Characterization of the Si-Sn nanocomposites. (A) XRD pattern and (B-C) SEM images of Si-Sn nanocomposites.

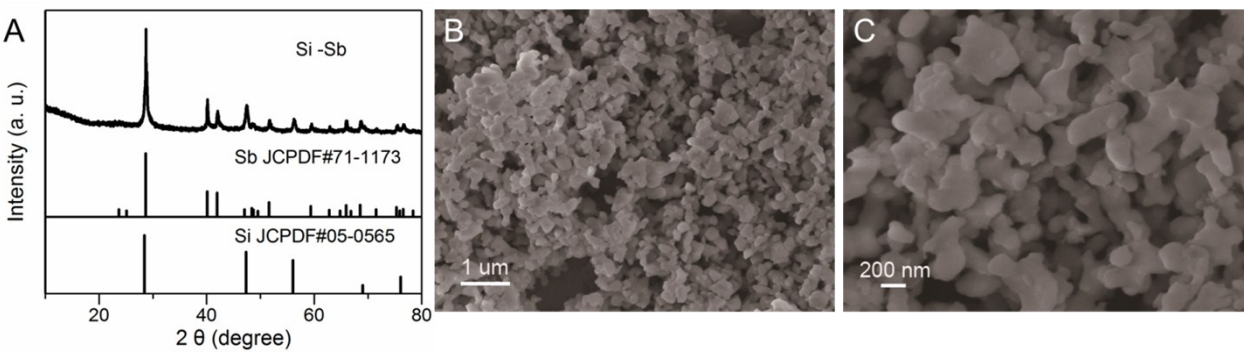


**Fig. S9** Characterization of the Si-Sb nanocomposites. (A) XRD pattern and (B-C) SEM images of Si-Sb nanocomposites.

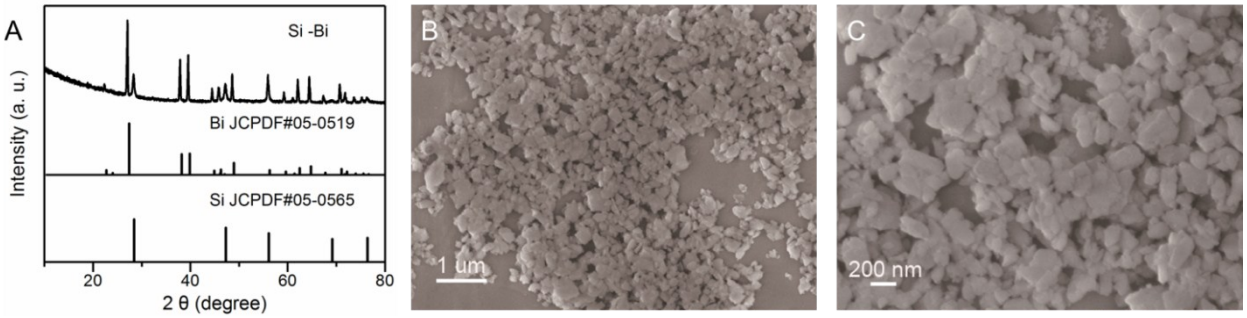


**Fig. S10** Characterization of the Si-Bi nanocomposites. (A) XRD pattern and (B-C) SEM images of Si-Bi nanocomposites.

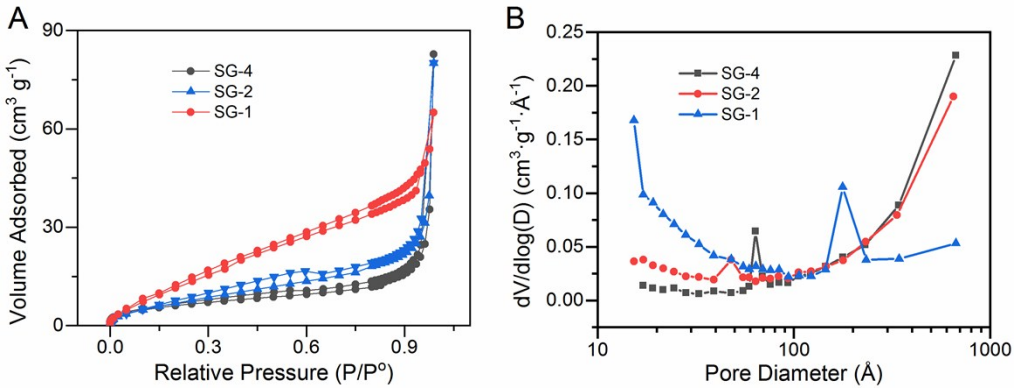


**Fig. S11** (A) Nitrogen adsorption-desorption isotherms of the SG-4, SG-2 and SG-1. (b-d) corresponding pore size distribution curves obtained by the BJH method.

The specific surface area of SG-4, SG-2 and SG-1 is 23, 27 and 50 m2 g-1, respectively.

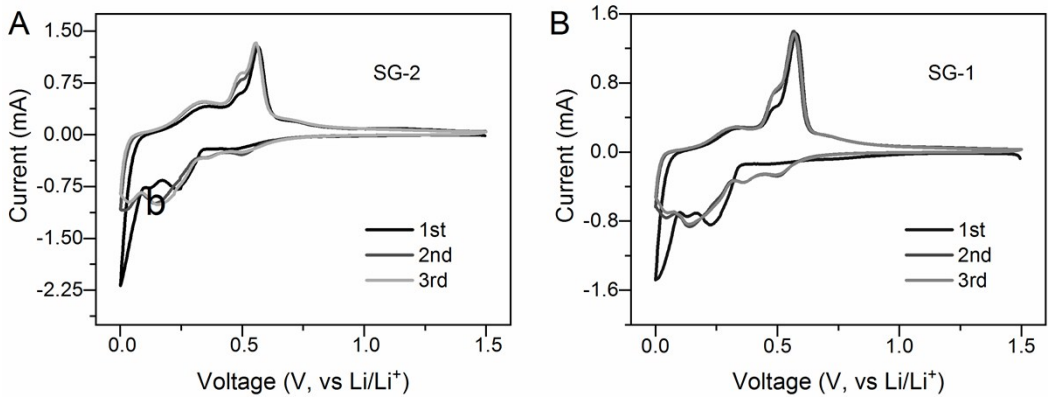


**Fig. S12** CV curves of the (A) SG-2 and (B) SG-1.

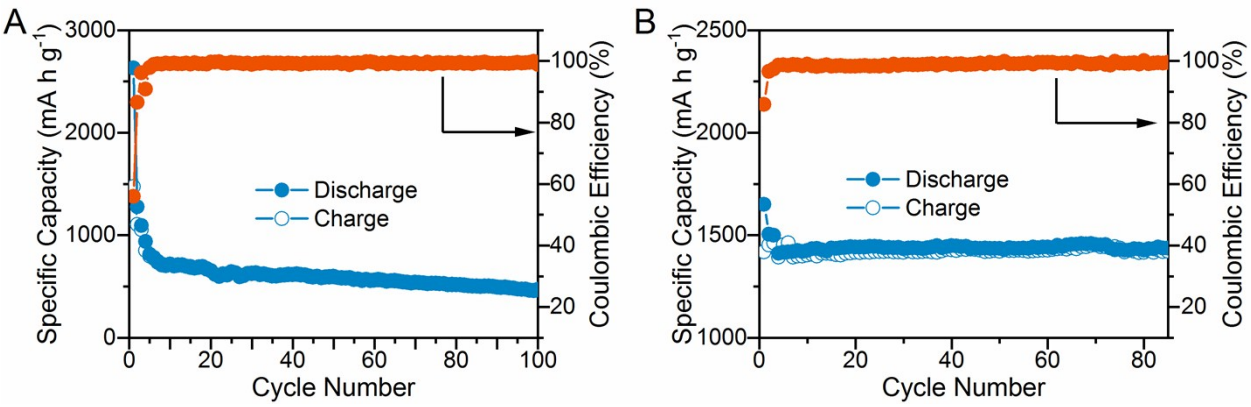


**Fig. S13** Cycling performance of (a) the mixture of Ge and Si and (b) Ge at the current density of 0.5 A $g^{-1}$.

**Table S3**. The comparison of electrochemical performance with other Si or Ge anodes reported in literatures.

| Si or Ge anodes | Reversible capacity (mAh $g^{-1}$) | Current density (mA $g^{-1}$) | Cycle number (cycles) | Ref. |
|---|---|---|---|---|
| 3D nanoporous SiGe alloy $Si_{12}Ge_8$ | 1372 | 100 | 80 | ACS Nano 2018, 12, 2900-2908. |
| Axial Si−Ge Heterostructure Nanowires | 1100 | 200 | 400 | Nano letters, 2018, 18(9): 5569-5575. |
| SiGe alloy nanotubes | 590 | 100 | 200 | Angew. Chem. Int. Ed. 2016, 55, 7427-7431. |
| Si nanoparticles | 3083 | 1200 | 50 | Angew. Chem. Int. Ed. 2015, 54, 1 – 5 |
| MXene-Si-CNT | ~1000 | 500 | 200 | ACS Nano, 2019, 13(8): 8854-8864. |
| C-Ge/C | 896 | 320 | 120 | Angew. Chem. Int. Ed. 2012, 51, 1 – 6 |
| $GeO_2$/Ge/C | 1650 | 2100 | 50 | Nano Letters, 2013, 13(3): 1230-1236. |
| Ge@CC | 1065.2 | 800 | 200 | Adv. Energy Mater. 2016, 6, 1501666 |
| SG-1 | 1493.4 | 500 | 150 | This work |
| SG-4 | 1615.8 | 500 | 150 | This work |

**Table S4**. voltage polarization of SG-4, SG-2 and SG-1 in voltage profile during rate tests.

| Current density (A $g^{-1}$) | 0.2 | 0.5 | 1 | 2 | 3 | 5 | 7 | 10 | 15 | 20 |
|---|---|---|---|---|---|---|---|---|---|---|
| SG-4 | 0.21 | 0.29 | 0.30 | 0.36 | 0.37 | 0.43 | 0.53 | 0.66 | 0.92 | 1.13 |
| SG-2 | 0.22 | 0.28 | 0.29 | 0.30 | 0.32 | 0.35 | 0.36 | 0.40 | 0.51 | 0.58 |
| SG-1 | 0.23 | 0.25 | 0.27 | 0.28 | 0.29 | 0.32 | 0.34 | 0.37 | 0.42 | 0.54 |

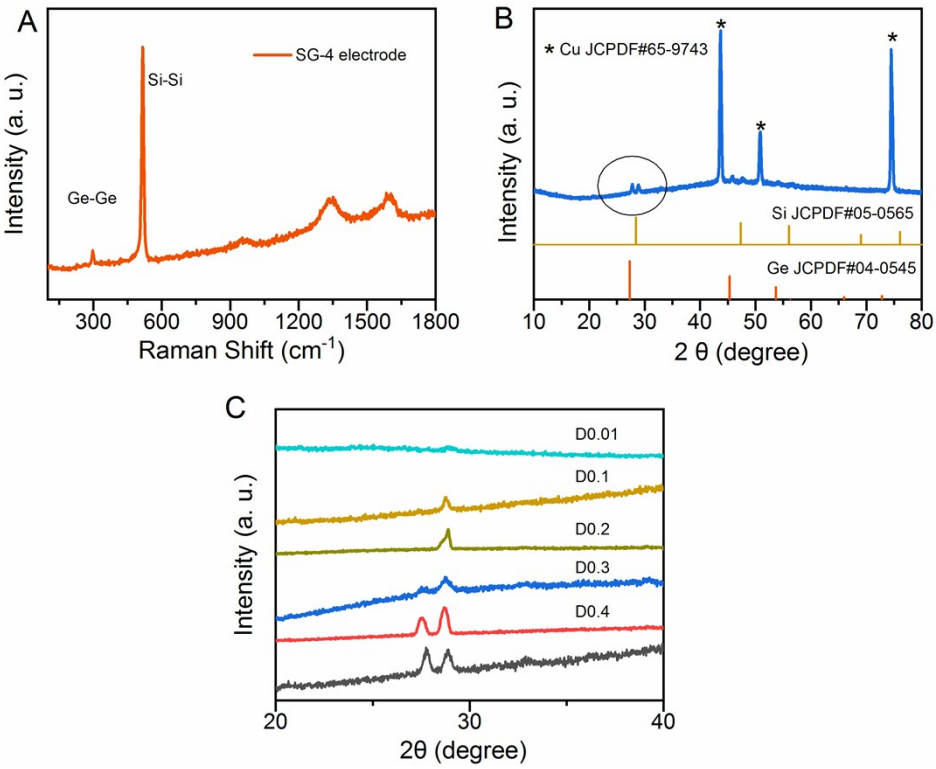


**Fig. S14** Ex situ XRD patterns between 20° and 40° of the SG-4 electrode at different potentials during lithium process.

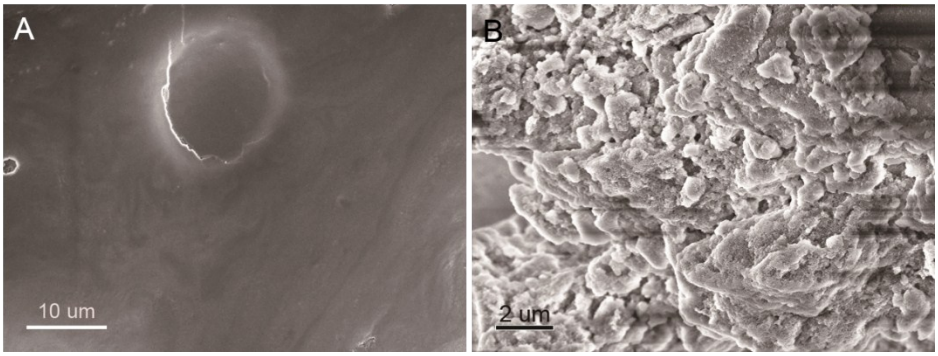


**Fig. S15** SEM image of Si-Ge electrode after 100 cycles at the current density of 0.5 A $g^{-1}$.

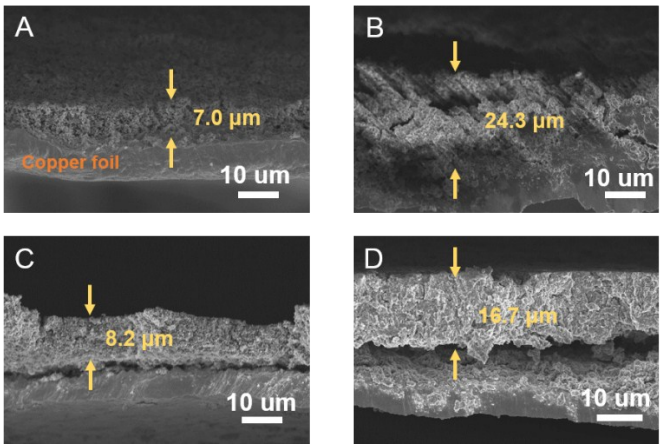


**Fig. S16** Cross-sectional view of the Si electrode (A) before cycling (B) after 50 cycles and Cross-sectional view of the Si-Ge electrode (C) before cycling (D) after 50 cycles.

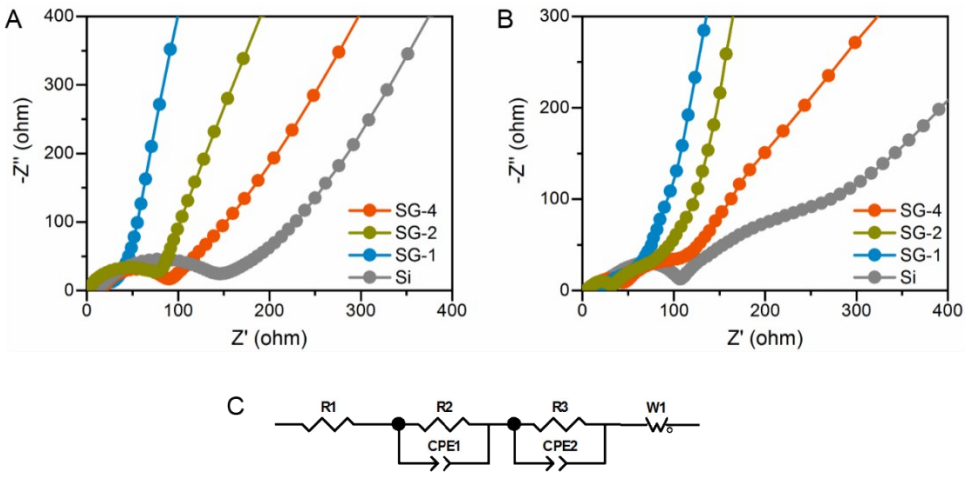


**Fig. S17** (A-B) Nyquist plots obtained for the cell of the Si-Ge and Si electrode, (A) before cycling (B) after 50 cycles and (C) equivalent circuit to model the impedance spectra.

**Table S5.** Simulated kinetic parameter of Si and Si-Ge electrode.

| | | R1 (Ω) | R2 (Ω) | R3 (Ω) |
|---|---|---|---|---|
| SG-1 | before | 1.30 | | 38.28 |
| | After 50 cycles | 5.50 | 18.15 | 32.50 |
| SG-2 | before | 2.04 | | 70.56 |
| | After 50 cycles | 4.88 | 24.48 | 69.80 |
| SG-4 | before | 9.57 | | 75.26 |
| | After 50 cycles | 8.28 | 36.75 | 86.8 |
| Si | before | 11.73 | | 138.0 |
| | After 50 cycles | 7.73 | 97.60 | 323.5 |

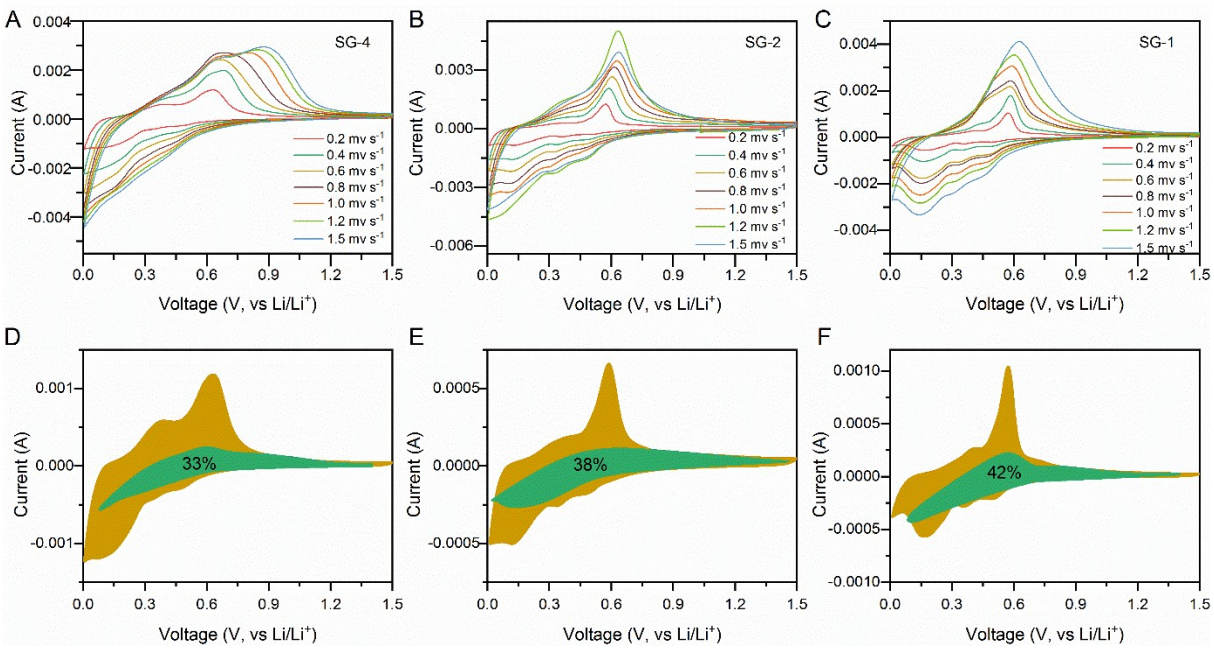


**Fig. S18** CV curves of SG-4 (B) SG-2 and (C) SG-1 electrode at different scan rates.

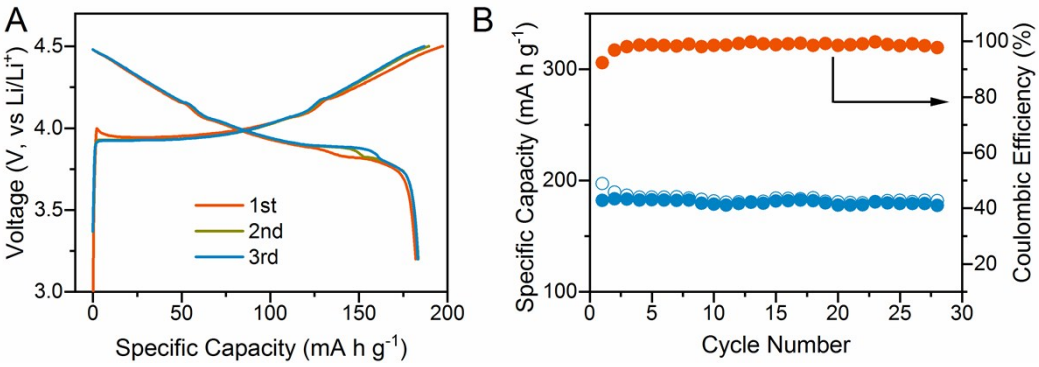


**Fig. S19** (A) voltage profile of the first three cycles and (B) cycling performance of the $LiCoO_2$ cathode.